

Near-field beam displacement at surface plasmon resonance

J.-C. Weeber, G. Colas-des-Francis, A. Bouhelier, and A. Dereux

*Laboratoire Interdisciplinaire Carnot de Bourgogne, UMR 5209 CNRS-Université de Bourgogne**9 avenue A. Savary, BP 47870, F-21078 Dijon, France*

(Received 2 September 2010; revised manuscript received 10 November 2010; published 16 March 2011)

A finite-size beam exciting a surface plasmon polariton (SPP) in a prism coupling configuration experiences an in-plane displacement that can be used for the characterization of plasmonic components by means of near-field optical microscopy. We first demonstrate experimentally the existence of this displacement by taking near-field images of finite-width metal strips. Next, the properties of this shift are analyzed in detail. We investigate the dynamic of the near-field shift for an incident Gaussian beam as a function of illumination conditions. For beams with a narrow spectrum, we propose a straightforward derivation showing that the displacement depends on the average angle of incidence according to a Lorentzian law characteristic of the SPP resonance. For smaller beams with typical sizes of an order or smaller than the plasmon damping distance, we give a heuristic expression relating the beam displacement to the amount of incident energy that can couple to the SPP mode. By using an analogy with tunneling experiments through a dielectric barrier, we demonstrate a direct-space analog of the Hartman effect. Finally we show that the beam displacement is a convenient parameter that can be used to optimize SPP mode excitation in plasmonic waveguiding geometries.

DOI: [10.1103/PhysRevB.83.115433](https://doi.org/10.1103/PhysRevB.83.115433)

PACS number(s): 73.20.Mf, 07.79.Fc, 78.66.–w

I. INTRODUCTION

Near-field optical microscopes operating in the collection mode are very convenient for the characterization of plasmonic components. On the other hand, a very popular way to achieve the excitation of nonlocal surface plasmon modes is to use an evanescent field produced in an attenuated total reflection or Kretschmann-Raether (K-R) configuration.¹ It is then important to fully understand the features visible in near-field images of plasmonic devices excited by a finite-size beam in the K-R configuration. Since the first near-field imaging of surface plasmon polariton (SPP) locally excited^{2,3} in this configuration, the technique has been used in many situations.^{4–7} However, so far only little attention has been paid to the behavior of the incident beam itself.

The shift of a finite-size beam incident on a dielectric stack was extensively investigated theoretically in the early 1970s.^{8,9} More recently this displacement has been considered when the beam illuminates negative index metamaterials,¹⁰ a simple metallic surface without SPP excitation,¹¹ a dielectric tunnel barrier,¹² or a lossy guiding geometry.¹³ Whatever the situation, the displacement of the reflected or transmitted beam (when it exists) is related to the angular dispersion of the phase of the reflection or transmission coefficient for the system under consideration. Such an angular dispersion of the phase occurs when a leaky wave is excited in the system but the existence of such a leaky wave is not necessary to observe a shift as in the case of the Goos-Hänchen (G-H) shift, for example.

The excitation of SPP modes by a finite-size beam has also been considered theoretically many years ago.^{14–16} The shaping of the reflected beam resulting from the excitation of long-range surface plasmon modes has been described theoretically in the spatial¹⁷ and temporal¹⁸ domains. The beam displacement at SPP resonance has also been observed experimentally for the reflected beam in the case of short surface plasmon modes excited in the far-infrared¹⁹ or for long-range surface plasmon modes.²⁰ More recently the

reflected beam shaping at SPP resonance for visible frequencies has been reported experimentally,^{21,22} and a SPP sensor based on the measurement of this displacement have been proposed and demonstrated.²³ However, in most of these works, the reflected beam was considered, and more importantly the incident beam was always large compared to either the SPP mode propagation distance or the incident wavelength, a situation that is only of small experimental interest for near-field experiments where a local launching of the SPP modes is often needed. In this work we focus specifically on the “transmitted” “beam in the near-field zone in the case of spot size as small as a few incident wavelengths. We show that the information encoded into the in-plane displacement can be useful for the characterization of plasmonic structures by near-field optical microscopy.

We first demonstrate experimentally the beam displacement at surface plasmon resonance by recording near-field images over finite-width metal strips. Next, we discuss the dynamic of the beam displacement as a function of the illumination conditions. For beams with sizes much larger than the SPP damping distance, we expose a simple approach showing that the displacement depends upon the average angle of incidence and follows a Lorentzian function characteristic of the SPP resonance. For smaller beams, we give a heuristic expression connecting the displacement to the amount of energy of the incident beam that can couple to the SPP mode. In the fourth section, we use an analogy with the “tunneling time” measured in tunneling experiments, to show that the beam displacement at SPP resonance exhibits a saturation for decreasing SPP losses that correspond to a direct space observation of the so-called Hartman effect. Finally, we demonstrate numerically in the fifth section how the in-plane shift can be used practically to optimize the excitation of dielectric loaded SPP waveguides.

II. EXPERIMENTAL DEMONSTRATION

The direct observation of the near-field beam displacement at surface plasmon resonance can be achieved by using a

near-field optical microscope operated in the collection mode, such as the photon-scanning tunneling microscope (PSTM). In this work, we used the setup described in Ref. 5 except for the near-field probe, which comprises a pure dielectric pulled single-mode fiber instead of a metal-coated multimode fiber. The observation of the near-field beam displacement at SPP resonance is possible only if the incident spot and the SPP mode are visible simultaneously on a single near-field image. For this reason, we consider the excitation of an SPP mode supported by a simple metal strip of finite width.^{5,6} Gold strips with a width of $2.5 \mu\text{m}$ and a height of 100 nm have been prepared by standard electron beam lithography and lift-off process. Figure 1(a) displays a typical PSTM image recorded over one of these metal strips when excited by a focused spot in the K-R configuration (incident free-space wavelength 800 nm). The TM polarized focused spot produced by a lensed-fiber has a waist of about $6 \mu\text{m}$. Although the incident spot is laterally shifted with respect to the metal strip, one can observe clearly the incident spot and the SPP mode excited onto the metal strip propagating from the top to the bottom of the near-field image. The dark contrast visible at the location of the incident spot for observation points situated right above the strip indicates a weak SPP excitation in this area. The

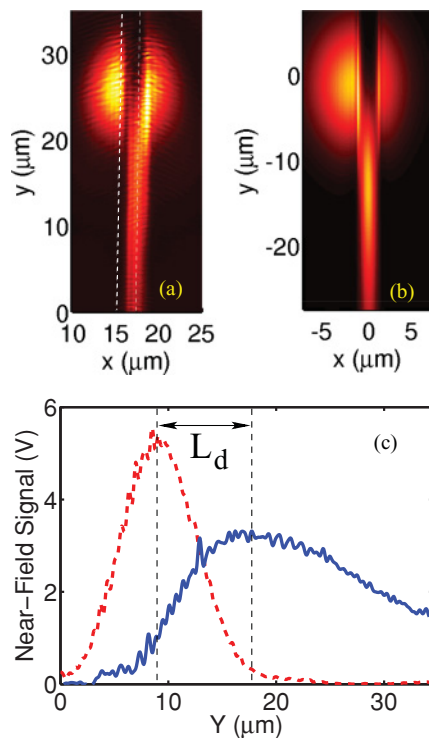


FIG. 1. (Color online) (a) Experimental near-field optical (PSTM) image showing the local excitation of a SPP mode onto a gold strip (width = $2.5 \mu\text{m}$, thickness = 100 nm) using a focused beam in the Kretschmann configuration. The incident spot (incident free-space wavelength = 800 nm) has a waist of roughly $6 \mu\text{m}$. (b) Electric field intensity distribution computed with the differential method at a distance of 50 nm above a gold strip excited in the Kretschmann configuration by a Gaussian beam. (c) Cross-cuts of the experimental images taken along the two dashed lines displayed in image (a). The beam displacement associated with the SPP excitation is denoted as L_d .

dashed and the solid curves displayed in Fig. 1(c) correspond, respectively, to the cross-cuts of the near-field image taken along the lines located on the left and at the center of the metal strip. From these profiles, we conclude that the centroid of the incident spot is “displaced” by a distance $L_d = 9 \mu\text{m}$. We note the very good agreement of the experimental image with the electric field intensity distribution [Fig. 1(b)] computed with the differential method^{24–26} in an observation plane located at a distance of 50 nm from the top of the metal strip. The “delayed” excitation of the SPP mode visible on the experimental and numerical near-field images was anticipated several decades ago¹⁹ and is demonstrated here by direct near-field imaging for what we believe to be the first time. The properties of this beam displacement are analyzed in the next section.

III. DYNAMIC OF THE BEAM DISPLACEMENT

We investigate in this section the dynamic of the near-field beam displacement as a function of the excitation conditions of the SPP mode. To that aim, we turn to the basic plasmonic situation depicted in Fig. 2(a). A two-dimensional TM polarized Gaussian beam traveling through a substrate (dielectric function ϵ_1) falls onto a metal thin film (thickness h) at an angle θ_i and excites a SPP mode at the metal/superstrate ($\epsilon_3 < \epsilon_1$) interface. In the local frame attached to the beam, the incident

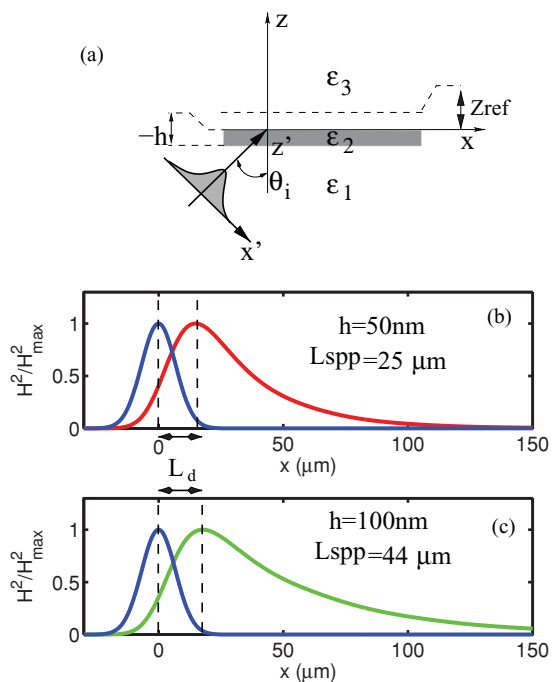


FIG. 2. (Color online) (a) Computational situation for the excitation of a SPP mode onto an extended thin film by a two-dimensional Gaussian beam. (b) [resp. (c)] Normalized magnetic intensity $\|H_y(x,z)\|^2$ profiles computed at a distance $Z_{\text{ref}} = 50 \text{ nm}$ from the top interface of a gold film with a thickness $h = 50 \text{ nm}$ (resp. $h = 100 \text{ nm}$). The incident wavelength is $\lambda_0 = 800 \text{ nm}$ ($n_{\text{gold}} = 0.180 + i5.12$). The profiles centered around $x = 0$ correspond to the incident magnetic field computed at $z = Z_{\text{ref}}$ in the absence of the metal film.

magnetic field is given by the plane wave expansion [temporal dependence $\exp(-i\omega t)$ assumed]:

$$H_y^i(x', z') = \int_{-\infty}^{+\infty} d\alpha \frac{w_0}{2\sqrt{\pi}} \exp\left(-\frac{w_0^2}{4}\alpha^2\right) \exp i(\alpha x' + \gamma^{(1)} z'), \quad (1)$$

where α is the wavevector component along the local frame direction x' and w_0 is the beam waist in the plane $z' = 0$, $\gamma^{(1)} = \sqrt{\varepsilon_1 k_0^2 - \alpha^2}$ with $k_0 = \frac{2\pi}{\lambda_0}$. Using this expansion, it is straightforward to obtain the magnetic field transmitted through the thin film as

$$H_y^i(x, z) = \int_{-\infty}^{\infty} dk_{\parallel} t^{(\text{TM})}(k_{\parallel}) H_y^i(k_{\parallel}) \exp i(k_{\parallel} x + k_z^{(3)} z), \quad (2)$$

where $k_{\parallel} = \alpha \cos \theta_i + \gamma^{(1)} \sin \theta_i$, $k_z^{(3)} = \sqrt{\varepsilon_3 k_0^2 - k_{\parallel}^2}$, and $t^{(\text{TM})}(k_{\parallel}) = |t^{(\text{TM})}(k_{\parallel})| \exp i\phi_t(k_{\parallel})$ is the TM Fresnel transmission coefficient through the metallic slab. From Eq. (2), it is clear that the excitation of a SPP mode with a finite-size beam has two effects on the beam spectrum. First, the beam is reshaped as a result of the wave-vector filtering imposed by the $|t^{(\text{TM})}(k_{\parallel})|$ coefficient, and, second, each plane wave of the Fourier expansion is dephased according to $\phi_t(k_{\parallel})$. Figure 2 shows the incident beam profile ($w_0 = 10 \mu\text{m}$, $\lambda_0 = 800 \text{ nm}$) along with the near-field profiles computed at $z = 50 \text{ nm}$ for a film thickness of $h = 50 \text{ nm}$ and $h = 100 \text{ nm}$. The near-field profiles exhibit the well-known plasmon tail resulting from the beam reshaping, but one can also observe a beam centroid displacement L_d of about $15 \mu\text{m}$ for $h = 50 \text{ nm}$ and $17 \mu\text{m}$ for $h = 100 \text{ nm}$. The lateral displacement is then almost constant, whereas the minimization of the radiation leakages causes the $1/e$ damping distance of the SPP field intensity (L_{spp}) to be much larger for $h = 100 \text{ nm}$ than for 50 nm . This simple example shows that there is a nontrivial dependence of the lateral shift upon the SPP damping distance. In order to analyze in a systematic way the dynamic of this shift, it is instructive to consider first beams with a waist very large compared to L_{spp} . These kinds of beams are denoted hereafter as quasilplane waves (QPWs).

A. Large beams

Although of moderate interest for near-field experiments, the situation of a SPP mode excited by a QPW is of great importance for understanding the properties of the beam displacement. We assume an incident QPW with a spectrum peaked at $k_{\parallel}^i = \sqrt{\varepsilon_1} k_0 \sin(\theta_i)$ and much narrower than the SPP resonance. For an average incident angle of the QPW closed to the air-metal SPP mode, the Fresnel transmission coefficient through the thin film can be written for each plane wave of the expansion of the QPW as^{9,27}

$$t(k_{\parallel}) = \frac{C \exp i\phi_c}{(k_{\parallel} - k_{\text{sp}})}, \quad (3)$$

where C and ϕ_c are slowly varying real functions of k_{\parallel} . The above pole approximation of $t(k_{\parallel})$ has been used by several authors in the same context to simplify the expression of $t(k_{\parallel})$.^{15,19} However, this equation is also very convenient to

express directly the phase of $t(k_{\parallel})$. Noting $k_{\text{sp}} = k_{\text{sp}}' + ik_{\text{sp}}''$, the phase $\phi_t(k_{\parallel})$ is given by

$$\phi_t(k_{\parallel}) = \arctan \frac{k_{\text{sp}}''}{(k_{\parallel} - k_{\text{sp}}')} + \phi_c. \quad (4)$$

Following the approach of Ref. 9 but applied to $\phi_t(k_{\parallel})$, we write the phase as a first-order Taylor expansion for k_{\parallel} close to k_{\parallel}^i :

$$\phi_t(k_{\parallel}) = \phi_t(k_{\parallel}^i) + (k_{\parallel} - k_{\parallel}^i) \phi_t'(k_{\parallel}^i). \quad (5)$$

Introducing Eq. (5) in Eq. (2) leads to

$$H_y^i(x, z) = \exp(i\delta) \int dk_{\parallel} |t^{(\text{TM})}(k_{\parallel})| H_y^i(k_{\parallel}) \times \exp i(k_{\parallel}(x + \phi_t'(k_{\parallel}^i)) + k_z^{(3)} z), \quad (6)$$

where $\delta = \phi_t(k_{\parallel}^i) - k_{\parallel}^i \phi_t'(k_{\parallel}^i)$ is a constant coefficient. The expansion (6) indicates that if the incident beam is peaked at $x = 0$, the transmitted beam will be peaked at $x = -\phi_t'(k_{\parallel}^i)$, leading directly to the conclusion that $-\phi_t'(k_{\parallel}^i)$ represents the in-plane displacement of the incident QPW. This result emphasizes that, unlike the reflected beam where the profile results from an interference between a specularly reflected and radiated fields,^{15,17-19} the lateral displacement for the transmitted beam at SPP resonance has strictly the same physical origin as the G-H shift.¹⁹ Indeed, replacing $t(k_{\parallel})$ in the above discussion by the reflection coefficient of a simple interface gives the well-known Artmann's formula²⁸⁻³⁰ for the G-H shift. From Eq. (4), we find that the displacement of the transmitted QPW is given by the Lorentzian function characteristic of the SPP resonance:

$$L_d = -\phi_t'(k_{\parallel}^i) = \frac{k_{\text{sp}}''}{(k_{\parallel}^i - k_{\text{sp}}')^2 + (k_{\text{sp}}'')^2}. \quad (7)$$

In the synchronous case $k_{\parallel}^i = k_{\text{sp}}'$, we retrieve the result of Ref. 16, $L_d = \frac{1}{k_{\text{sp}}''}$, obtained in the context of a dielectric stack that can also be written in our case as

$$L_d = 2 \times L_{\text{spp}}. \quad (8)$$

In principle, it is then possible to measure the damping distance of a SPP mode even though the beam size prohibits the direct observation of the SPP damping on near-field images. From an experimental point of view, this result can be useful for measuring the propagation distance of highly damped SPP modes excited by an evanescent field. Indeed, in this situation, the observation of the plasmon tail is difficult as it requires a very local excitation, whereas the displacement of beams large compared to L_{spp} can be easily extracted from optical near-field images recorded over standard scanning sizes of a few tenths of microns.

The phase of $t(k_{\parallel})$ for a gold film of $h = 50 \text{ nm}$ along with the power spectrum of a beam (waist $w_0 = 150 \lambda_0$) are plotted in Fig. 3(a). As expected for any resonance phenomenon, the phase ϕ' experiences a jump (close to π if the losses of the SPP mode are small)^{18,27} when k_{\parallel} crosses the resonance condition. This phase jump introduces a phase shift causing, respectively (at least for sufficiently large beams), a destructive and constructive interference at the trailing and front edges of

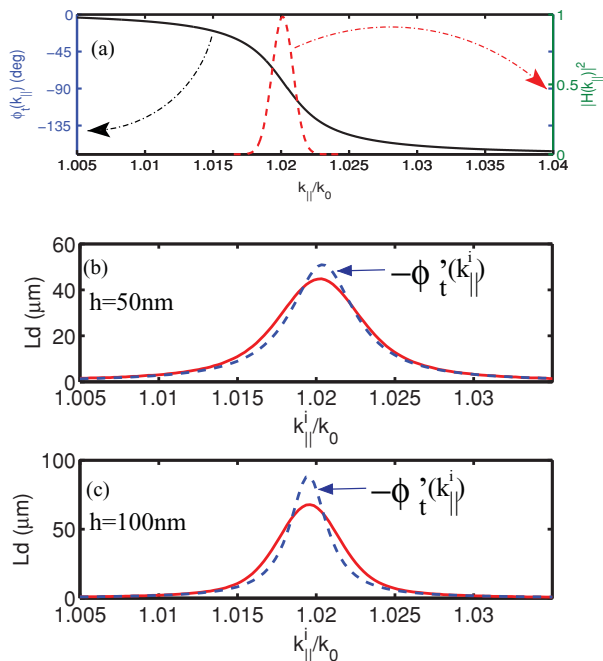


FIG. 3. (Color online) (a) (left frame axis) Phase of the transmission Fresnel coefficient for a gold film (thickness of 50 nm) supported by a glass substrate illuminated by a plane wave with a wavelength of $\lambda_0 = 800$ nm. (right frame axis) Power spectrum of a Gaussian beam with a waist of $w_0 = 120 \mu\text{m}$. (b) [resp. (c)] (solid line) Numerically evaluated in-plane displacement of a Gaussian beam ($w_0 = 120 \mu\text{m}$) illuminating a gold film with a thickness of 50 nm (resp. 100 nm) as a function of the angle of incidence. (dashed line) In-plane displacement of the beam evaluated using Eq. (7).

the beam. Figures 3(b) and 3(c) show the change of in-plane displacement with respect to the angle of incidence in the case of a Gaussian beam with a waist of $w_0 = 150 \lambda_0$ illuminating gold films of respective thicknesses of 50 and 100 nm. For $h = 50$ nm, the displacement fits fairly well with the lateral shift computed from Eq. (7) showing that a nonresonant ($k_{\parallel}^i \neq k_{\text{spp}}^i$) excitation of SPP mode leads to a strong decrease of the beam displacement. In the case $h = 100$ nm, the beam displacement is clearly different from that given by Eq. (7). In this case, the discrepancy arises from the fact that the reduced radiation leakages resulting from the thicker (100 nm) film cause the SPP resonance to be narrower than in the case of the 50 nm film. For the thick film, the beam spectrum is not narrow enough compared to the SPP resonance for the pole approximation of Eq. (3) to be accurate. In such a situation, one must then account carefully for the spectrum width of the incident beam.

It is worth noting that the process prevailing at the shaping of large beams at SPP resonance holds also in the case of a plane wave exciting a thin film with a finite width.³¹ In this last case the finite size of the incident beam is imposed by the metal film itself. For example, the near-field magnetic profiles computed for a plane wave exciting a SPP mode on a finite-width gold film ($w = 40 \mu\text{m}$, $h = 50$ nm) and a rectangular beam illuminating an infinite thin film¹⁵ are shown for two angles of incidence in Fig. 4(c) and 4(d). If the finite film is resonantly excited [Fig. 4(c)], the evanescent coupling

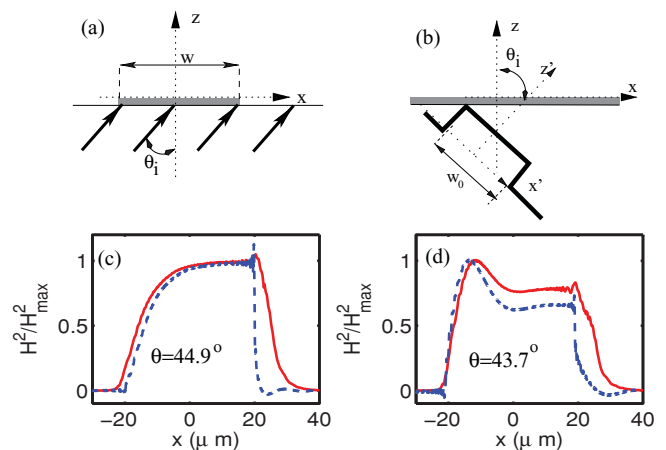


FIG. 4. (Color online) Computational situations: (a) Finite-width film illuminated by a plane wave. (b) Extended thin film excited by a finite-width rectangular beam. The incident wavelength is $\lambda_0 = 633$ nm ($n_{\text{gold}} = 0.180 + i2.99$). (c) For a resonant angle of incidence $\theta = 44.9^\circ$: comparison of the near-field profiles corresponding to situation (a) with $w = 40 \mu\text{m}$ (dashed line) and (b) with $w_0 = 23 \mu\text{m}$ (solid line). Note that for an optimum comparison in the resonant case, the value $w_0 = 23 \mu\text{m}$ is chosen slightly smaller than $w \cos \theta = 24.3 \mu\text{m}$ in order to account for the divergence of the incident rectangular beam making the beam larger in the observation plane than in the focal plane. (d) Same as (c) except for the angle of incidence $\theta = 43.7^\circ$.

excitation dominates over the scattering excitation, and the SPP field intensity exhibits a profile similar to the trailing edge of the SPP mode excited on the extended thin film by the rectangular beam. If the angle of incidence is slightly off-resonance [Fig. 4(d)], the contribution of the scattering channel for the excitation of the SPP mode on the finite film increases, and in turn, the agreement with the rectangular beam excitation profile degrades. From these observations we conclude that for a resonant excitation, the phase and the amplitude of the plane waves in the Fourier expansion of the field diffracted by the finite film (illuminated by an incident plane wave) is imposed by the SPP resonance itself, provided, however, that the diffracted field spectrum is narrow compared to the SPP resonance.

B. Intermediate and small beams

In most near-field experiments, the beam used for local excitation of plasmonic structures is necessarily smaller than L_{spp} and possibly as small as a few incident wavelengths. There is no simple way to assess analytically the beam displacement when its spectrum is broad. Indeed, adding nonlinear terms in the Taylor expansion of the phase leads to an analytical result only at the price of the use of the paraxial approximation, which holds for spot sizes very large compared to the incident wavelength.^{9,15,32} Recalling the origin of the beam displacement detailed in the previous paragraph, it is reasonable to associate a “displacement” $-\phi_t'(k_{\parallel})$ to each plane wave of the beam spectrum. Given that the contribution to the beam displacement of a plane wave with a vanishing amplitude should be small, we express the displacement of

the beam itself as a weighted average of the displacement of each plane wave according to

$$L_{\text{av}} = \frac{\int_{-\infty}^{\infty} -|H^{\text{inc}}(k_{\parallel})|^2 \phi'_i(k_{\parallel}) dk_{\parallel}}{\int_{-\infty}^{\infty} |H^{\text{inc}}(k_{\parallel})|^2 dk_{\parallel}}. \quad (9)$$

We compare in Fig. 5(a) the value of the beam displacement obtained numerically and computed with the heuristic Eq. (9) for incident beams of different sizes resonantly coupled to the SPP mode sustained by a 50 nm- or 100 nm-thick gold film. As expected, we observe the saturation of the beam displacement to twice the SPP damping distance for large beams. For smaller spots, we note a fairly good agreement between L_d and L_{av} . In particular, the strong decrease of L_d with the spot size is well accounted for by Eq. (9).³³ Figure 5(b) shows the incident and transmitted field intensity profiles computed in the case of a beam with a waist of $w_0 = 2.0 \mu\text{m}$ for an incident wavelength of $\lambda_0 = 800 \text{ nm}$. The transmitted profile exhibits a pronounced distortion due to the low-pass filtering imposed by the SPP resonance in agreement with the observation of SPP excitation by tightly focused beams.³⁴ In addition, we note that for beams much smaller than L_{spp} the displacement is always close to $w_0 / \cos \theta_i$ as a combined result of the abrupt decrease

of the incident field amplitude at the front edge of the beam and the poor SPP coupling.

The interest of Eq. (9) lies mainly in the fact that it provides a direct interpretation of the dynamic of the beam displacement. Indeed, L_{av} is obtained from an overlap integral of the power spectrum of the incident beam and the SPP resonance characterized by the Lorentzian function of Eq. (7). Thus, the displacement L_{av} is proportional to the amount of incident energy carried by the plane waves that can couple to the SPP mode normalized by the energy carried by the whole plane wave spectrum. On the basis of this result, the decrease of L_d for resonant beams with decreasing waist is straightforward since a small waist corresponds to a broad spectrum that overlaps only a little with the SPP resonance. Finally, the same argument can be used to explain the decrease of L_d for a beam with a given waist and an off-resonance average angle of incidence. Based on this discussion, we note that an increase of L_d can always be attributed to an improved coupling to the SPP mode.

IV. BEAM DISPLACEMENT AND SPP MODE PROPERTIES: HARTMAN EFFECT

We have considered so far the dynamic of the beam displacement for given SPP modes and changing illumination conditions (angle of incidence and beam waist). However, it is also interesting to analyze the beam displacement in the case of given illumination conditions and changing SPP mode properties.

The beam displacement at SPP resonance has long been recognized as a build-up process;¹⁹ *i.e.*, the incident field must interact with the SPP mode over a sufficient distance to accumulate energy in it. This unambiguous interpretation of the beam displacement is rather straightforward in our case where the SPP mode participating to the beam displacement is clearly identified. It is nevertheless very useful to understand the results obtained in the context of “tunneling times” measurements where the lack of such a clear interpretation has been at the origin of intense debate. When a finite-size beam tunneled through a barrier comprising a low index slab sandwiched between two high-index media, it experiences a spatial lateral shift³⁵ that has long been interpreted as a propagation distance leading to “superluminal” group velocity values during a tunneling process. To resolve this paradox, it has been suggested^{36,37} that the group delay related to this lateral shift should not be interpreted as a transit time but rather as a cavity lifetime provided that the duration of the incident pulse is long enough. In complete analogy with this last interpretation, we have shown in our case that for a beam large enough, the lateral shift is characteristic of the SPP mode ($L_d = 2L_{\text{spp}}$), the SPP mode in our situation playing the role of the cavity mode in tunneling experiments. Recalling that the beam displacement at SPP resonance for the transmitted beam (and only for the transmitted beam) is an analog to the G-H shift (causing the beam displacement in tunneling experiment), it is licit to extrapolate the results obtained for the transmitted field at SPP resonance to the situation of a dielectric tunnel barrier.

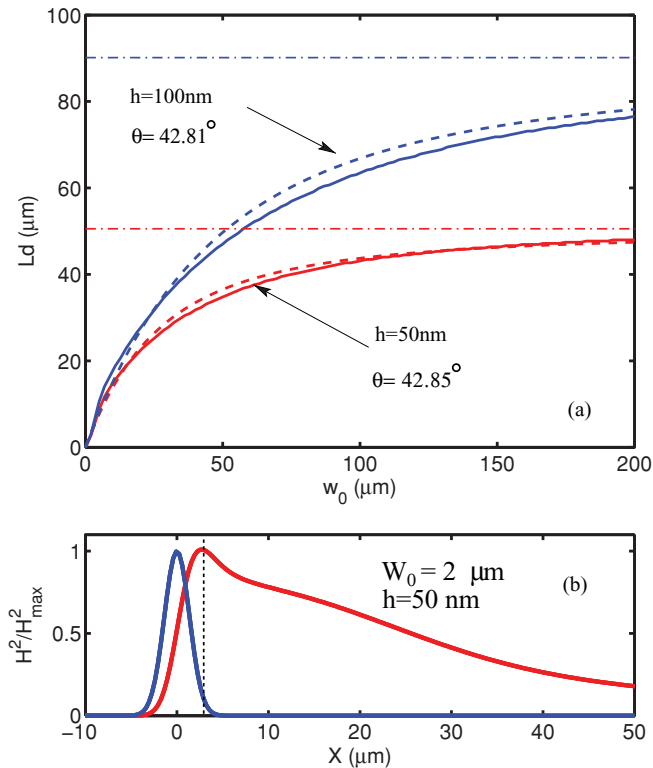


FIG. 5. (Color online) (a) (solid lines) Change of the in-plane displacement for Gaussian beams with increasing waists exciting resonantly a SPP mode on gold films (thickness h). (dashed lines) Near-field in-plane displacement of the beam evaluated using Eq. (9). The dash-dotted lines correspond to twice L_{spp} for $h = 50 \text{ nm}$ and $h = 100 \text{ nm}$. (b) Incident and transmitted magnetic field intensity profiles computed for an incident beam with $w_0 = 2.0 \mu\text{m}$ (incident wavelength $\lambda_0 = 800 \text{ nm}$).

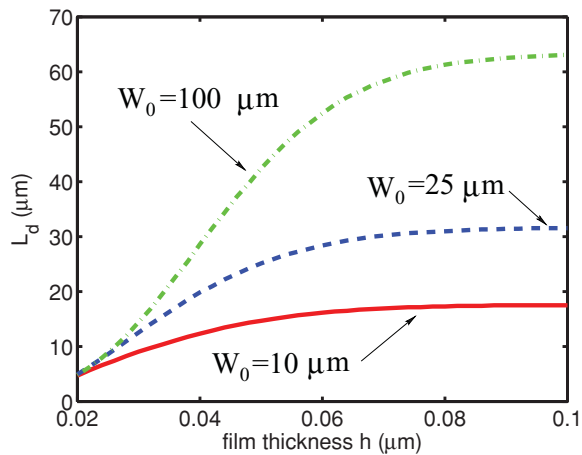


FIG. 6. (Color online) Saturation of the in-plane displacement for Gaussian beams exciting a SPP mode on gold films of increasing thicknesses. The saturation results from a minimization of the losses of the SPP mode. The saturation value depends upon the beam waist of the incident beam.

Pushing further the analogy, we can define a “build-up time” of the SPP mode directly from the expression of the beam displacement. For large w_0 we have

$$L_d = -\frac{d\phi_t}{dk_{\parallel}} = -\frac{d\phi_t}{d\omega} \frac{d\omega}{dk_{\parallel}} = -\frac{d\phi_t}{d\omega} v_g = \tau_d v_g, \quad (10)$$

where τ_d is the build-up time and v_g the group velocity of the SPP mode. Given that $L_d = 2 \times L_{\text{spp}}$, one finds $\tau_d = 2 \times \tau_{\text{spp}}$ where $\tau_{\text{spp}} = L_{\text{spp}}/v_g$ is the lifetime of the SPP mode. From this simple approach, we conclude that a pulse (with a large spatial extension) will be delayed by twice the SPP lifetime at SPP resonance provided that the incident pulse duration is long enough (compared to τ_{spp}). Such a delay could be observed, for example, by time-resolved near-field experiments.^{38,39} Transposing the dynamic of the beam displacement from the direct space to the temporal domain, one can immediately anticipate that if the incident pulse duration is decreased, the build-up time will also be reduced, leading to a smaller SPP excitation. Finally, we note that unlike the reflected beam, the time delay at SPP resonance for the transmitted field is not expected to change dramatically the temporal profile of the incident pulse.¹⁸

When the width of a tunnel barrier is increased, the group delay (phase time) or equivalently the lateral shift of the incident beam exhibits a saturation. This effect is known as the Hartman effect.⁴⁰ In our case, the increase of the tunnel barrier width corresponds to an increase of the metal thin film thickness. Figure 6 shows the change of L_d for different spot sizes and film thicknesses. As expected from the tunneling experiments we also observe a saturation of the beam displacement, which is just the transposition to the direct space of the Hartman effect. The origin of this saturation can be understood directly by considering once again the case of very large beams. In this case we have $L_d = \frac{1}{k_{\text{spp}}''}$, hence the saturation of L_d originates from the saturation of k_{spp}'' , which can be explained by the vanishing contribution of the radiation leakages to the total losses when the metal film thickness increases. If the spot size is not large compared

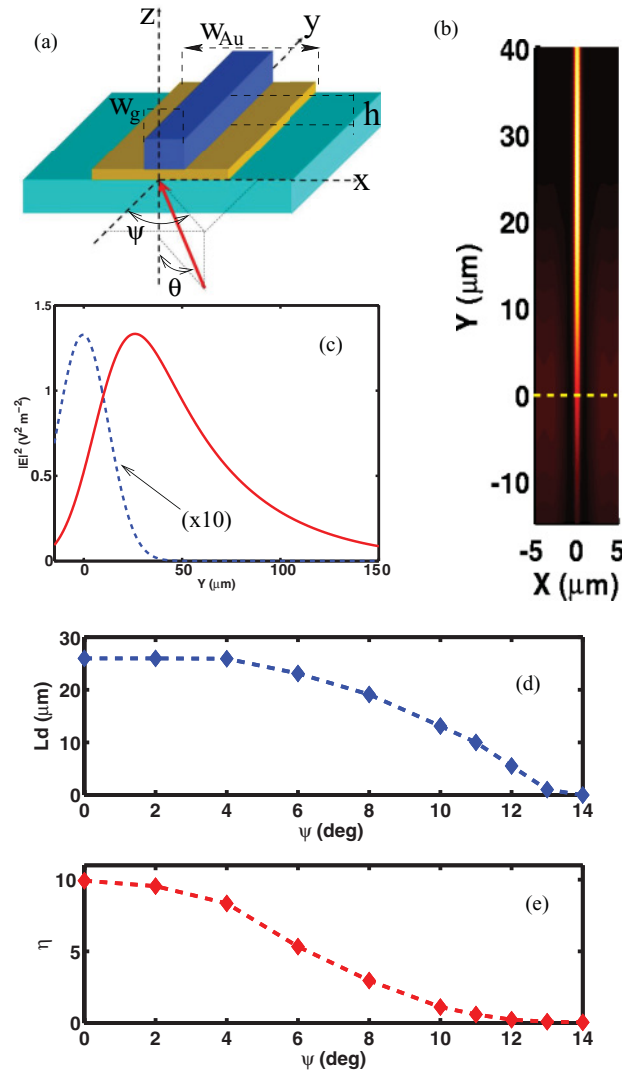


FIG. 7. (Color online) (a) Definition of the parameters describing the excitation of a DLSPW by a cylindrical Gaussian beam. The illumination direction is controlled by the incident angle θ and the azimuthal angle ψ . (b) Near-field electric field intensity distribution computed in a plane located 50 nm over the top of the DLSPW (see text for parameters). The angle of incidence is fixed to $\theta = 54.2^\circ$ and $\psi = 0^\circ$. The underneath gold strip is 3 μm wide. The dashed line shows the location of the centroid of the incident beam. (c) Longitudinal cross-cuts of the near-field intensity map taken over the spot (dashed line) and along the DLSPW (solid line). (d) In-plane displacement for different azimuthal angles. (e) Enhancement factor as a function of the azimuthal angle.

to L_{spp} , the saturation of L_d still occurs. However, in this case the saturation value is no more characteristic of the SPP mode alone (although the saturation of L_d still originates from a decrease of the SPP mode losses) and can be computed for a given w_0 by using Eq. (9).

V. APPLICATION TO DIELECTRIC LOADED SPP WAVEGUIDES

The measurements of the reflected beam displacement at SPP resonance in the far-field zone can be used to determine the damping distance of the SPP mode.^{15,17,19,23} In the near-field

zone, the SPP damping distance can be *a priori* measured directly. In this context, the practical interest of L_d is more in the optimization of SPP coupling than in the measurement of L_{spp} . In this section we demonstrate numerically such an optimization in the case of dielectric loaded SPP waveguides (DLSPPWs), i.e., polymer waveguides loaded on top of a metal film or strips that have been found to be of interest for short passive or active waveguiding applications.^{41–43} Figure 7(a) shows a typical DLSPP waveguide comprising a dielectric ridge (index = 1.5, waveguide width $w_g = 560$ nm, waveguide height $h = 500$ nm) deposited on top of a gold strip (thickness = 80 nm) with a width w_{Au} . The DLSPPW is excited in the Kretschmann configuration by a TM polarized Gaussian beam with a frequency corresponding to a free-space wavelength of $\lambda_0 = 1.55$ μm and having a waist of $w_0 = 15$ μm . The illumination conditions of the DLSPPW are controlled by the incidence angle θ and the azimuthal angle ψ . Using the definitions of θ and ψ given in Fig. 7(a), the central plane wave in the expansion of the incident Gaussian beam has a wavevector component along the DLSPPW axis (y axis) given by $k_y = k_0 \sin \theta \cos \psi$. The optimum excitation of the DLSPP mode is expected when k_y matches the longitudinal wavevector component of the guided mode. Thus, the optimization of the DLSPPW excitation imposes the adjustment of not only the angle of incidence θ but also the azimuthal angle ψ , which controls the misalignment of the plane of incidence with the waveguide axis. From an experimental point of view, adjusting the incidence angle can be done by focusing the incident spot on a polymer film area. Assuming that the effective index of the SPP mode for the polymer film and the DLSPPW are not too different, the optimum angle of incidence is adjusted simply by looking at the dark arc of circle in the reflected spot characterizing the plasmon mode excitation. However, for the azimuthal angle such an adjustment is no longer possible, since a wide polymer film does not help to control the in-plane propagation direction of the SPP mode. In the case of a near-field characterization of the DLSPPW, the adjustment of the azimuthal angle can be performed by optimizing the intensity measured above the waveguide or alternatively by maximizing the lateral displacement of the beam centroid. Figure 7(b) shows an electric near-field intensity map computed with the differential method in an observation plane located at 50 nm from the top of the DLSPPW when the azimuthal angle is $\psi = 0^\circ$. The DLSPPW mode excitation makes difficult the observation of the incident spot centered at $Y = 0$; however, by taking a cross-cut along the longitudinal axis of the waveguide and over the incident spot we observe a pronounced displacement of about 26 μm [Fig. 7(c)]. The same computation has been performed for increasing values of ψ . For a given azimuthal angle, we compute L_d and the enhancement factor η defined as $\eta = \frac{E_{\text{max}}^2(\text{SPP})}{E_{\text{max}}^2(\text{inc})}$, where $E_{\text{max}}^2(\text{SPP})$ and $E_{\text{max}}^2(\text{inc})$ denote the

maximum intensity for the SPP mode and the incident spot in the same observation plane. The in-plane displacement and the enhancement factor are, respectively, displayed on Figs. 7(d) and 7(e). We observe that the two quantities follow the same trend in agreement with the discussion of the second section. Thus, we conclude that the optimization of the plasmonic waveguides excitation can be conducted by direct measurement of the beam displacement rather than by the maximization of the near-field intensity.

VI. CONCLUSION

In summary, we have investigated the near-field displacement of a finite-size beam exciting a SPP mode in the Kretschmann configuration in the context of near-field optical microscopy.

Based on an approximate expression of the SPP field phase, we have established that the displacement of quasi-plane waves depends on the angle of incidence according to a Lorentzian law characteristic of the SPP resonance. This displacement saturates to twice the damping distance of the SPP mode for resonant beams. By considering the overlap of the SPP resonance and the power spectrum of the incident beam, we note that the beam displacement decreases proportionally to the amount of incident energy that can be coupled to the SPP mode. Thus, for a given SPP mode, the increase of L_d is always indicative of an improved coupling as shown by the results obtained for a simple thin film or a DLSPP waveguide.

The displacement of the transmitted beam at SPP resonance has the same origin as the G-H shift. In this respect, the dynamic of the displacement in the presence of SPP modes with different damping distances can be used to interpret tunneling experiments through a dielectric barrier. In particular, the Hartman effect has been demonstrated in direct space by the saturation of the beam displacement L_d when the damping of the SPP mode reaches a minimum, whatever the origin of loss minimization. From this observation we conclude that, for given illumination conditions, the saturation of L_d is characteristic of SPP mode properties, although the value of L_d at saturation depends on the illumination conditions. Finally, beyond the fundamental properties of SPP mode launching by finite-size evanescent fields, the beam displacement provides useful information for the analysis of near-field images of plasmonic waveguides. In particular, the optimization of SPP mode coupling, which is primary a matter of intensity measurements, is transformed into a simple beam displacement measurement that can be readily performed by near-field optical microscopy.

ACKNOWLEDGMENTS

This work has been supported by the European STREP Project PLATON (Grant 249135-FP7-ICT-2009-4).

¹H. Raether, *Surface Plasmon on Smooth and Rough Surfaces and on Gratings* (Springer-Verlag, Berlin, 1986).

²P. Dawson, F. de Fornel, and J.-P. Goudonnet, *Phys. Rev. Lett.* **72**, 2927 (1994).

³P. Dawson, B. A. F. Puygranier, and J.-P. Goudonnet, *Phys. Rev. B* **63**, 205410 (2001).

⁴J.-C. Weeber, J. R. Krenn, A. Dereux, B. Lamprecht, Y. Lacroute, and J.-P. Goudonnet, *Phys. Rev. B* **64**, 045411 (2001).

- ⁵J.-C. Weeber, Y. Lacroute, and A. Dereux, *Phys. Rev. B* **68**, 115401 (2003).
- ⁶R. Zia, J. A. Schuller, and M. L. Brongersma, *Phys. Rev. B* **74**, 165415 (2006).
- ⁷T. Holmgaard, S. I. Bozhevolnyi, L. Markey, A. Dereux, A. V. Krasavin, P. Bolger, and A. V. Zayats, *Phys. Rev. B* **78**, 165431 (2008).
- ⁸T. Tamir and H. L. Bertoni, *J. Opt. Soc. Am.* **61**, 1397 (1971).
- ⁹C. W. Hsue and T. Tamir, *J. Opt. Soc. Am. A* **2**, 978 (1985).
- ¹⁰G. Dolling, M. W. Klein, M. Wegener, A. Schädle, B. Kettner, S. Burger, and S. Linden, *Opt. Express* **15**, 14219 (2007).
- ¹¹M. Merano, A. Aiello, G. W.'t Hooft, M. P. Exter, E. R. Eliel, and J. P. Woerdman, *Opt. Express* **15**, 15928 (2007).
- ¹²X. Chen, C-F. Li, R.-R. Wei, and Y. Zhang, *Phys. Rev. A* **80**, 015803 (2009).
- ¹³J. Hao, H. Li, C. Yin, and Z. Cao, *J. Opt. Soc. Am. B* **27**, 1305 (2010).
- ¹⁴S. L. Chang, *J. Opt. Soc. Am. A* **3**, 593 (1986).
- ¹⁵E. F. Y. Kou and T. Tamir, *Appl. Opt.* **28**, 1169 (1989).
- ¹⁶V. Shah and T. Tamir, *J. Opt. Soc. Am. A* **73**, 37 (1983).
- ¹⁷R. T. Deck, D. Sarid, G. A. Olson, and J. M. Elson, *Appl. Opt.* **22**, 3397 (1983).
- ¹⁸R. V. Alvarado, H. J. Simon, and R. T. Deck, *Appl. Opt.* **33**, 6340 (1994).
- ¹⁹W. P. Chen, G. Ritchie, and E. Burstein, *Phys. Rev. Lett.* **37**, 993 (1976).
- ²⁰R. A. Booman, G. A. Olson, and D. Sarid, *Appl. Opt.* **25**, 2729 (1986).
- ²¹X. Yin, L. Hesselink, Z. Liu, N. Fang, and X. Zhang, *Appl. Phys. Lett.* **85**, 372 (2004).
- ²²H. J. Simon, R. V. Andaloro, and R. T. Deck, *Opt. Lett.* **32**, 1590 (2007).
- ²³X. Yin and L. Hesselink, *Appl. Phys. Lett.* **89**, 261108 (2006).
- ²⁴Michel Nevière and Evgeny Popov, *Light Propagation in Periodic Media, Differential Theory and Design* (Marcel Dekker, New York, 2003).
- ²⁵M. U. González, J.-C. Weeber, A.-L. Baudrion, A. Dereux, A. L. Stepanov, J. R. Krenn, E. Devaux, and T. W. Ebbesen, *Phys. Rev. B* **73**, 155416 (2006).
- ²⁶S. Massenot, J.-C. Weeber, A. Bouhelier, G. Colas-des-Francis, J. Grandidier, L. Markey, and A. Dereux, *Opt. Express* **16**, 17599 (2008).
- ²⁷E. Anemogiannis, E. N. Glytsis, and T. K. Gaylord, *J. Lightwave Technol.* **17**, 929 (1999).
- ²⁸C.-F. Li and Q. Wang, *Phys. Rev. E* **69**, 055601(R) (2004).
- ²⁹J. D. Jackson, *Classical Electrodynamics*, 3rd ed. (John Wiley, Hoboken, NJ, 1999), p. 342.
- ³⁰C.-F. Li, *Phys. Rev. A* **76**, 013811 (2007).
- ³¹L. Salomon, G. Bassou, H. Aourag, J. P. Dufour, F. de Fornel, F. Carcenac, and A. V. Zayats, *Phys. Rev. B* **65**, 125409 (2002).
- ³²X. Chen, C-F. Li, R-R. Wei, and Y. Zhang, *Phys. Rev. A* **80**, 015803 (2009).
- ³³The agreement between L_d and L_{av} degrades for small beams when the excitation is not resonant ($k_{\parallel}^i \neq k'_{spp}$). This is due to the fact that in this case one should account for nonlinear terms in the Taylor expansion of the phase $\phi'(k_{\parallel})$. For resonant beams, ($k_{\parallel}^i = k'_{spp}$), the contribution of these nonlinear terms vanishes because the second derivative $\phi''(k_{\parallel})$ is odd with respect to k'_{spp} explaining why we still observe a good agreement between L_d and L_{av} for small resonant beams.
- ³⁴A. Bouhelier, F. Ignatovitch, A. Bruyant, C. Huang, G. Colas des Francis, J.-C. Weeber, A. Dereux, G. P. Wiederrecht, and L. Novotny, *Opt. Lett.* **32**, 2535 (2007).
- ³⁵P. Balcou and L. Dutriaux, *Phys. Rev. Lett.* **78**, 851 (1997).
- ³⁶H. G. Winful, *Opt. Express* **10**, 1491 (2002).
- ³⁷H. G. Winful, *Phys. Rep.* **436**, 1 (2006).
- ³⁸M. L. M. Balistreri, H. Gersen, J. P. Korterik, L. Kuipers, and N. F. Van Hulst, *Science* **294**, 1080 (2001).
- ³⁹H. Gersen, T. J. Karle, R. J. P. Engelen, W. Bogaerts, J. P. Korterik, N. F. van Hulst, T. F. Krauss, and L. Kuipers, *Phys. Rev. Lett.* **94**, 073903 (2005).
- ⁴⁰T. E. Hartman, *J. Appl. Phys.* **33**, 3427 (1962).
- ⁴¹T. Holmgaard, Z. Chen, S. I. Bozhevolnyi, L. Markey, A. Dereux, A. V. Krasavin, and A. V. Zayats, *Opt. Express* **16**, 13585 (2008).
- ⁴²T. Holmgaard, Z. Chen, S. I. Bozhevolnyi, L. Markey, and A. Dereux, *Opt. Express* **17**, 2968 (2009).
- ⁴³J. Grandidier, G. Colas des Francis, S. Massenot, A. Bouhelier, L. Markey, J.-C. Weeber, C. Finot, and A. Dereux, *Nano Lett.* **9**, 2935 (2009).